The Astrophysical Journal Letters, 922:L42 (9pp), 2021 December 1 https://doi.org/10.3847/2041-8213/ac34fd

The Remarkable Spin-down and Ultrafast Outflows of the Highly Pulsed Supersoft Source of Nova Herculis 2021

Jeremy J. Drake[1], Jan-Uwe Ness[2], Kim L. Page[3], G. J. M. Luna[4,5,6], Andrew P. Beardmore[3], Marina Orio[7,8], Julian P. Osborne[3], Przemek Mróz[9,10], Sumner Starrfield[11], Dipankar P. K. Banerjee[12], Solen Balman[13,14], M. J. Darnley[15], Y. Bhargava[16], G. C. Dewangan[16], and K. P. Singh[17]

[1] Harvard-Smithsonian Center for Astrophysics, 60 Garden Street, Cambridge, MA 02138, USA; jdrake@cfa.harvard.edu
[2] European Space Agency (ESA), European Space Astronomy Centre (ESAC), Camino Bajo del Castillo s/n, E-28692 Villanueva de la Cañada, Madrid, Spain
[3] School of Physics & Astronomy, University of Leicester, Leicester LE1 7RH, UK
[4] CONICET-Universidad de Buenos Aires, Instituto de Astronomía y Física del Espacio (IAFE), Av. Inte. Güiraldes 2620, C1428ZAA, Buenos Aires, Argentina
[5] Universidad de Buenos Aires, Facultad de Ciencias Exactas y Naturales, Buenos Aires, Argentina
[6] Universidad Nacional de Hurlingham, Av. Gdor. Vergara 2222, Villa Tesei, Buenos Aires, Argentina
[7] Department of Astronomy, University of Wisconsin–Madison, 475 N. Charter Street, Madison WI 53706, USA
[8] INAF-Padova, vicolo Osservatorio, 5, I-35122 Padova, Italy
[9] Division of Physics, Mathematics, and Astronomy, California Institute of Technology, Pasadena, CA 91125, USA
[10] Astronomical Observatory, University of Warsaw, Al. Ujazdowskie 4, 00-478 Warszawa, Poland
[11] Earth and Space Exploration, Arizona State University, P.O. Box 871404, Tempe, AZ 85287-1404, USA; starrfield@asu.edu
[12] Physical Research Laboratory, Ahmedabad, INDIA 380009
[13] Department of Astronomy and Space Sciences, Istanbul University, 34119 Istanbul, Turkey
[14] Faculty of Engineering and Natural Sciences, Kadir Has University, Cibali, 34083 Istanbul, Turkey
[15] Astrophysics Research Institute, Liverpool John Moores University, IC2 Liverpool Science Park, Liverpool L3 5RF, UK
[16] Inter-University Centre for Astronomy and Astrophysics, Ganeshkhind, Pune, 411 007, India
[17] Indian Institute of Science Education and Research Mohali, Sector 81, P.O. Manauli, SAS Nagar, 140 306, India
Received 2021 August 26; revised 2021 October 20; accepted 2021 October 25; published 2021 December 3

Abstract

Nova Her 2021 (V1674 Her), which erupted on 2021 June 12, reached naked-eye brightness and has been detected from radio to γ-rays. An extremely fast optical decline of 2 magnitudes in 1.2 days and strong Ne lines imply a high-mass white dwarf. The optical pre-outburst detection of a 501.42 s oscillation suggests a magnetic white dwarf. This is the first time that an oscillation of this magnitude has been detected in a classical nova prior to outburst. We report X-ray outburst observations from Swift and Chandra that uniquely show (1) a very strong modulation of supersoft X-rays at a different period from reported optical periods, (2) strong pulse profile variations and the possible presence of period variations of the order of 0.1–0.3 s, and (3) rich grating spectra that vary with modulation phase and show P Cygni–type emission lines with two dominant blueshifted absorption components at ~3000 and 9000 km s^{-1} indicating expansion velocities up to 11,000 km s^{-1}. X-ray oscillations most likely arise from inhomogeneous photospheric emission related to the magnetic field. Period differences between reported pre- and post-outburst optical observations, if not due to other period drift mechanisms, suggest a large ejected mass for such a fast nova, in the range 2×10^{-5}–$2 \times 10^{-4}\,M_{\odot}$. A difference between the period found in the Chandra data and a reported contemporaneous post-outburst optical period, as well as the presence of period drifts, could be due to weakly nonrigid photospheric rotation.

Unified Astronomy Thesaurus concepts: Novae (1127); Classical novae (251); Fast novae (530); X-ray novae (1818); DQ Herculis stars (407); X-ray astronomy (1810); X-ray transient sources (1852); Cataclysmic variable stars (203); White dwarf stars (1799); Stellar winds (1636)

1. Introduction

Nova Herculis 2021 (TCP J18573095+1653396, ZTF19aasfsjq, hereafter V1674 Her) is proving to be one of the most fascinating nova events so far during this young century. It was discovered on 2021 June 12.5484 UT, at an apparent visual magnitude of 8.4 by Seidji Ueda (Kushiro, Hokkaido, Japan)[18]; an earlier detection of June 12.1903 UT was subsequently reported by the All-Sky Automated Survey for Supernovae (ASAS-SN; Aydi et al. 2021). Later on the same day of discovery, the object was observed to reach a peak magnitude of approximately 6 (Munari et al. 2021; Quimby et al. 2021; see also AAVSO Alert Notice[19]), thus just visible to the unaided eye. Early spectroscopy indicated the object to be a very fast, reddened, classical nova (Munari et al. 2021; Aydi et al. 2021).

V1674 Her subsequently garnered copious attention from radio to γ-rays. Quimby et al. (2021) found an extremely fast decay timescale, t_2, of 2 magnitudes in only 1.2 days using high-cadence optical photometry, and a remarkable plateau in the pre-maximum light curve at 8 magnitudes below peak that lasted for 3 or more hours. Li (2021) found an uncataloged gamma-ray source at the nova position based on Fermi-LAT data in the 0.1–300 GeV range obtained on 2021 June

[18] http://www.cbat.eps.harvard.edu/unconf/followups/J18573095+1653396.html

[19] https://www.aavso.org/aavso-alert-notice-745

12.0–13.3. Sokolovsky et al. (2021) reported the detection of V1674 Her on 2021 June 15–17 at radio frequencies.

Optical and infrared spectroscopy showed P Cygni profiles in addition to flat-topped Balmer line profiles with substantial substructure and an increasing line width with time, with widths up to 11,000 km s^{-1} (Albanese et al. 2021; Balam et al. 2021; Aydi et al. 2021). Woodward et al. (2021a) reported the appearance of infrared coronal emission lines based on data obtained on 2021 June 24, while Wagner et al. (2021) observed strong [Ne V] λ3426 and [Ne III] λ3869,3968 coronal lines on 2021 June 30 and concluded that V1674 Her is a neon nova originating on an ONe white dwarf (WD); based on its rapid photometric decline, Wagner et al. (2021) also declared V1674 Her to be "the fastest nova on record."[20]

A monitoring program by the Neil Gehrels Swift Observatory (Swift) began on 2021 June 13.5. The nova was detected by the X-ray Telescope (XRT) on June 14.41 (day 2.22 after the ignition time of June 12.1903 based on the ASAS-SN data; Aydi et al. 2021) and a supersoft X-ray source (SSS) was seen to emerge on July 1 (day 18.9; Page et al. 2021). Swift UV observations were reported by Kuin et al. (2021).

Perhaps the most remarkable of the findings on V1674 Her is the detection of a 501.42 s periodic signal in archival *r*-band Zwicky Transient Facility (ZTF; Bellm et al. 2019) data collected between 2018 March 26 and 2021 June 14 (i.e., during pre-outburst quiescence) by Mroz et al. (2021). Shugarov & Afonina (2021) and Patterson et al. (2021) subsequently reported the detection of a 0.15302(2) day orbital period, with Patterson et al. (2021) also finding a 501.52 s period. Mroz et al. (2021) interpreted the 501 s period as the spin period of a WD in an intermediate polar system (IP).

IPs host a magnetized WD with a magnetic field of $10^{4\text{-}7}$ G and an accretion disk that is disrupted close to the WD by the magnetic field that channels accretion onto the polar caps from the disk at the magnetospheric radius (e.g., Patterson 1994; Wickramasinghe 2014; Mukai 2017). Thus, V1674 Her is the first such object whose magnetic nature was possibly revealed early in the outburst. This discovery prompted a Chandra Director's Discretionary Time (DDT) High Resolution Camera (HRC-S) X-ray photometric observation and the subsequent detection by Maccarone et al. (2021) of X-ray oscillations at a period of 503.9 s with an amplitude of 0.6 to 1.4 times the mean count rate. The oscillations were confirmed by Neutron Star Interior Composition Explorer (NICER) observations that found a period of 501.8 ± 0.7 s and that the count rate varied by up to a factor of $\sim$20 over a 20 minute observation (Pei et al. 2021). This result places V1674 Her in a small group of four novae in which modulations of the SSS flux over the likely rotation period of the WD were observed (V4743 Sgr, V2491 Cyg, and V407 Lup being the other three). Periodic modulation has been seen in an additional handful of sources, but the nature of those variations remains less clear.

The distance to V1674 Her is presently not well determined. Bailer-Jones et al. (2021) list $d = 6.0 \pm^{+3.8}_{-2.8}$ kpc based on Gaia EDR3. A distance of $d \sim 4.75$ kpc was found by Woodward et al. (2021b) using a variation of the maximum magnitude rate of decline (MMRD) method to derive the distance and extinction simultaneously. Currently, we adopt a nominal distance of 5 kpc.

[20] This indeed appears to be the case for Galactic novae, although we note that similarly fast candidates have been identified in M31 (e.g., Henze et al. 2014).

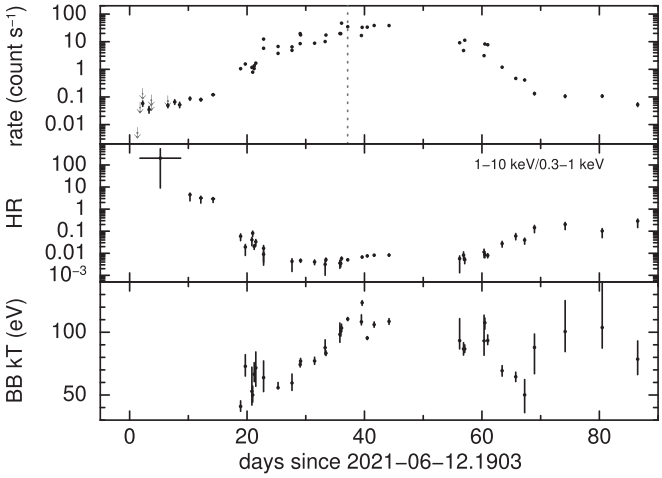

Figure 1. Swift-XRT 0.3–10 keV light-curve (top panel) and hardness ratio comparing the 1–10 and 0.3–1 keV bands (middle panel); a hardness ratio value <1 indicates that the SSS is dominating the emission. The bottom panel shows the BB temperatures from the fit described in the text. The arrows denote 3σ upper limits. The vertical dotted line marks the time of the Chandra observation.

Here, we present the first results of Swift X-ray monitoring observations and a second Chandra DDT observation of V1674 Her, this time made at high spectral resolution using the Low-Energy Transmission Grating (LETG) and HRC-S detector. We report the Swift observation details in Section 2, the Chandra observation and analysis in Section 3, before discussing and summarizing the results in Sections 4 and 5.

2. Swift Observations and Analysis

Swift observed V1674 Her typically every 1–2 days, from 1.3 days after the eruption, and continued up to day 44 (July 26); there was then a gap of 12 days, before regular observations resumed on day 56 (August 7). Given the optical brightness of the nova, most observations during the first 10 days were taken using the Windowed Timing (WT) mode of the XRT to help minimize the effect of optical loading.[21] Photon Counting mode was then used from days 10–29, before the source count rate again increased and required WT mode. Only single pixel (grade 0) events were considered throughout. Data were analyzed using HEASoft version 6.28 and the latest calibration files.

Spectra were extracted for each continuous snapshot of Swift data (typically 0.5–1 ks in duration) from the time when the SSS appeared (day 18.9) until the most recent observation, thus averaging over any variation caused by the periodicity.

2.1. X-Ray Light Curve

The early X-ray flux from V1674 Her was relatively faint and had a (1–10 keV)/(0.3–1.0 keV) hardness ratio HR > 1, likely due to optically thin emission. From day 18.9 a new supersoft component was seen below 1 keV. An exponential rise in the count rate followed, with superimposed short-term variations possibly due to the $\sim$500 s periodicity (Figure 1). The soft X-ray flux peaked around day 40.

[21] https://www.swift.ac.uk/analysis/xrt/optical_loading.php

2.2. Spectroscopic Analysis

Spectroscopic analysis of the Swift pulse-height spectra comprised model parameter estimation using the XSPEC fitting engine. A combination of an optically thin component (to model the underlying shock emission), and a blackbody (BB) together with absorption edges at 0.55, 0.67, 0.74, and 0.87 keV (corresponding to N VI, N VII, O VII, and O VIII, respectively) was used to model the spectra during the SSS phase; the BB component strongly dominated during this time. This model led to good fits, with reduced Cash statistic values of <1.5. We also examined fits to the `rauch_H-Ca_solar_90.fits` atmosphere grid,[22] which provided equally statistically acceptable results.

BB fits to the spectra indicated that the overall absorbing column remained constant, at a level of 2.9×10^{21} cm^{-2}, so fits were subsequently performed with $N_{\rm H}$ fixed at this value. Between days 18.9 and 27.7, the BB temperature remained approximately constant, at kT $\sim$54 eV; after this time, the emission steadily became hotter, reaching kT $\sim$ 130 eV (1.5×10^6 K; the highest SSS temperature for a Galactic nova seen by Swift to date) on day 39.6. At some point during the observing gap between days 44 and 56, the SSS phase started to fade and cool, reaching a minimum of $\sim$ 50 eV by day 67. After this time, the temperature started to increase again, returning to $\sim$100 eV by day 74.2. The BB temperatures are shown in the bottom panel of Figure 1.

During the SSS phase, the dominant absorption edges required to improve the BB fit changed. At the beginning, when the SSS temperature was lower, the edges at 0.55 and 0.67 keV were a significant improvement on the BB-only fit. As the BB temperature started to increase, these became less important, with the higher-energy 0.74 and 0.87 keV edges starting to dominate. We note that the trend of increasing and then decreasing BB temperature was also found if the spectra were fitted without absorption edges, and when using atmosphere model fits.

Comparison between the Chandra grating data (Section 3.2) and the approximately contemporaneous XRT observation shows a very similar overall spectral shape.

3. Chandra Observations and Analysis

V1674 Her was observed by Chandra using the LETG +HRC-S grating and detector combination. The observation began at 2021 July 19 UT07:40 (day 37.3 of the outburst) for a net exposure time of 29641 s. Data were analyzed using CIAO software version 4.13 with calibration database CALDB version 4.9.5.[23]

3.1. Timing Analysis

Light curves were first constructed from both the zeroth-order and the ±1 order (tg_m=1,−1) signals after applying barycentric corrections to photon arrival times. The extraction region for zeroth order was a circle of radius 3.8 arcsec while the default source and background region were used in the case of the ±1 orders. Background was negligible in comparison to the source signal. The zeroth-order light curve is illustrated in Figure 2.

In order to search for periodic signals, including near the $\sim$501.42 s signal found in the ZTF data (Mroz et al. 2021), we employed a Lomb–Scargle (LS) periodogram (Lomb 1976; Scargle 1982) and epoch folding. To determine the uncertainty in the period, 1000 light curves comprising a constant and sine wave with the same pulsed fraction, count rate, and 30 ks duration as observed by Chandra were analyzed. Each simulation corresponded to a different Poisson realization of the model. The recovered period had a standard deviation of 0.11 s.

Both zeroth- and first-order events were analyzed separately, each yielding the same result. The best-fit period from the zeroth-order data was 501.72 ± 0.11 s and is shown in Figure 2. This period is also close to the 503.9 s period reported for the initial Chandra HRC-S observation obtained on 2021 July 10 UT01:12 by Maccarone et al. (2021) and the 501.8 ± 0.7 s period reported from a NICER observation obtained between 2021 Jul 10 and 2021 July 12 (Pei et al. 2021). However, as we discuss later in Section 4.4, it is also likely different from the ZTF period reported by Mroz et al. (2021), and the period found by Patterson et al. (2021)

The zeroth-order light curve folded at the 501.72 s period is illustrated in Figure 2 and shows significant departures from a pure sine wave. A fourth-term LS periodogram shows power at ω, 2ω, 3ω, and 4ω with aliases of the main period at $\omega/2$, $\omega/3$, and $\omega/4$. We fit the light curve using a model including these harmonics in a Fourier series and sinusoidal components with frequencies that are integer multiples of the main frequency ω (VanderPlas 2018). The phase-folded light curve through the Chandra observation shows large variations in the pulse profile. This is also evident in the light curve in Figure 2. Using similar methods to the period search described above, we also searched for period variations within the observation to probe for period drifts or quasi-periodic oscillations (QPOs). Suggestive period variations were found at the level of $\sim$0.1-0.3 s. However, we were unable to verify their significance as variations were of a similar magnitude to uncertainties.

Phased light curves were also extracted for different wavelength ranges from the dispersed spectral orders. The pulsed fraction as a function of wavelength is also illustrated in Figure 2.

3.2. Spectroscopic Analysis

The first-order spectrum was extracted from the event list using the CIAO `tgextract` routine. Owing to the fairly narrow wavelength range of the bright spectrum, higher-order contamination of the first-order spectrum was negligible.

In the top panel of Figure 3, the spectrum of V1674 Her is shown with gray shadings. To put this spectrum into context, additional Chandra LETGS spectra of other bright nova SSS are overplotted for comparison: LMC 2012 (ObsID 14426), V407 Lup (ObsID 20632), and KT Eri (ObsID 12203), scaled with the factors given in the top right legend. The positions of some prominent spectral lines and ionization energies (edges) have been included. In the bottom panel, spectra extracted for the "high" and "low" phases highlighted in the phased light curve in Figure 2 are shown.

[22] http://astro.uni-tuebingen.de/~rauch/TMAF/flux_H-Ca.html
[23] https://cxc.harvard.edu/ciao/

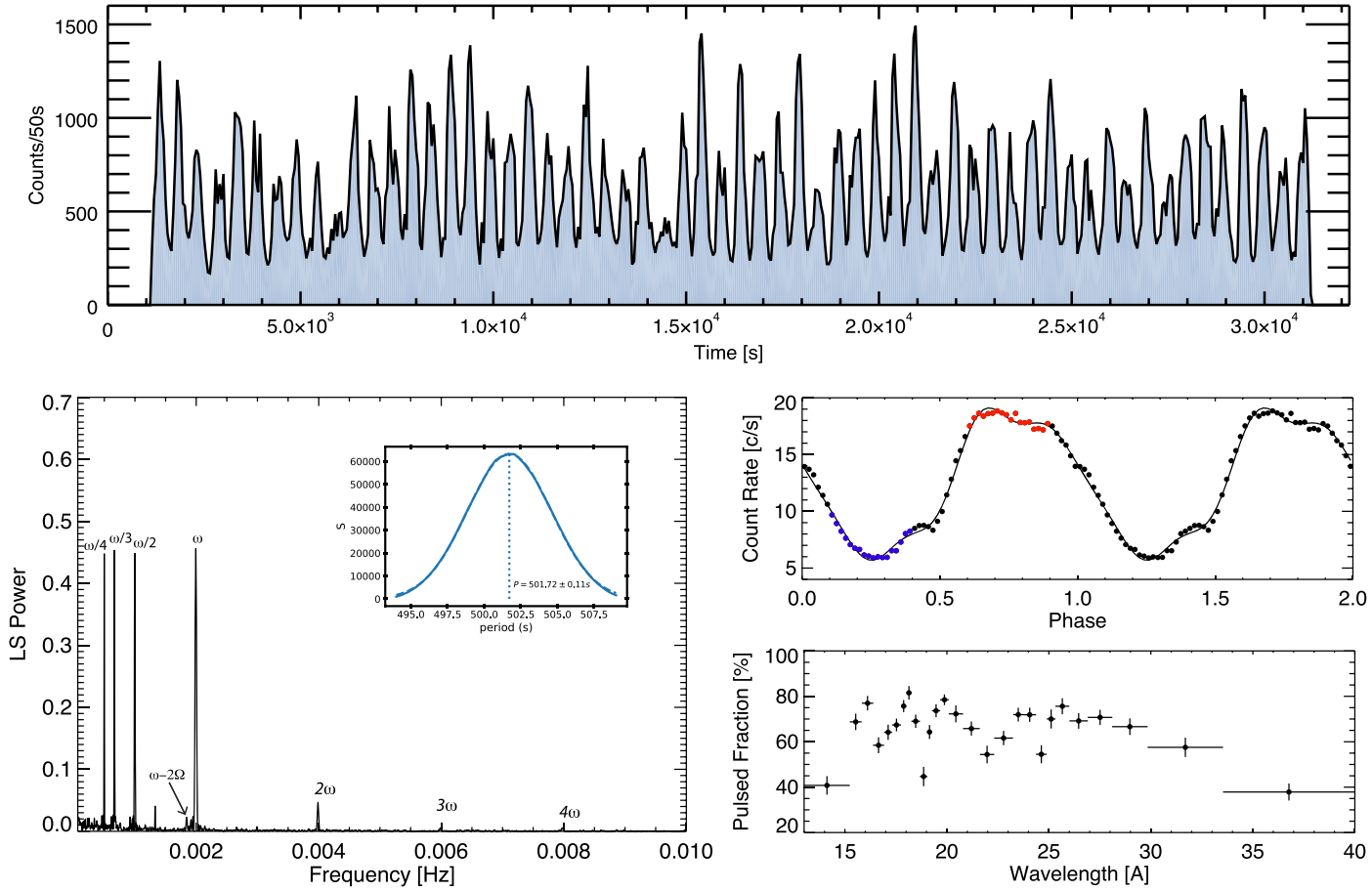

Figure 2. The timing analysis of the LETG+HRC-S observation of V1674 Her. Top: the HRC-S zeroth-order light curve in 50 s bins. Bottom left: the LS power spectrum of V1674 Her derived from the HRC-S zeroth-order light curve sampled with 1 s binning with some significant frequencies highlighted, including the ω-2Ω beat period reported by Patterson et al. (2021). The inset shows the χ^2 vs. period plane centered on the strongest peak of the power spectrum and a Gaussian fit to it. Bottom right (top): the light curve folded at a period of 501.72 s, with 40 bins/cycle and a fit of a model comprising a series of sine waves whose frequencies are integer multiples of the main frequency ω. Note that the error bars are smaller than the symbol size. The phase ranges for states deemed "high" and "low" for which phase-dependent spectra are extracted in Section 3.2 are highlighted with red and blue symbols, respectively. Bottom right (bottom): the pulsed signal fraction (defined as (max–min)/max in the count rate light curve) in different wavelengths derived from the dispersed ±1 order signal.

4. Discussion

4.1. V1674 Her Is a Very Fast Nova

With an optical decline from peak by 2 magnitudes in 1.2 days (Quimby et al. 2021), V1674 Her is classed as a very fast nova (one of the fastest known). Such rapid fading is commonly ascribed to a comparatively low mass of ejected gas (10^{-6}-$10^{-5} M_\odot$) at high velocity (up to 10,000 km s^{-1}; e.g., Gehrz et al. 1998), which itself arises from a low accreted mass at the time of eruption; for a low accreted mass, a high-mass WD is needed to achieve the pressure necessary for nuclear ignition (Starrfield et al. 2016, and references therein; see also Starrfield et al. 2020). A high WD mass is also indicated by the detection of optical Ne lines, leading Wagner et al. (2021) to propose that V1674 Her is an ONe WD, which is expected to have a mass >1.05 $M_\odot$ (Doherty et al. 2015; but see also Althaus et al. 2021).

A low ejecta mass and high ejecta velocity can be expected to lead to a rapid fall in the column density to the WD photosphere and thus a rapid emergence of the SSS, as was observed. First seen at 18.9 days after outburst, the SSS is in the fastest quartile to emerge among the Swift novae (Schwarz et al. 2011; Page et al. 2020).

The normalizations to model atmosphere and BB fits to the Swift spectra around the time of the Chandra observation indicated luminosities of approximately $L \sim 1 \times 10^{38}$ erg s^{-1} and 3×10^{37} erg s^{-1}, respectively, for a 5 kpc distance. A luminosity derived using a BB approximation to the SSS spectrum must be considered uncertain. However, the consistency between the BB and atmosphere model values to within a factor of a few lends modest support to the order of magnitude derived. The SSS emission is then essentially at the Eddington Limit ($L = 1.26 \times 10^{38}$ erg s^{-1} for a $\sim$1 $M_\odot$ WD; the actual limit will be lower for SSS emission because the gas is not fully ionized).

4.2. Phase-dependent X-Ray Emission

There are two potential explanations for the periodic modulation of the SSS X-ray emission. As noted in Section 1, Maccarone et al. (2021) have interpreted the modulation as being due to the spin period of the WD. Before addressing that, we also note that g-mode pulsations could be responsible. Indeed, some hints of g-mode pulsations during the SSS phase of other novae were reported by Drake et al. (2003) and Leibowitz et al. (2006), and the periodicity that is present both before and after the thermonuclear runaway (TNR), is a reasonable g-mode period (Starrfield et al. 1984).

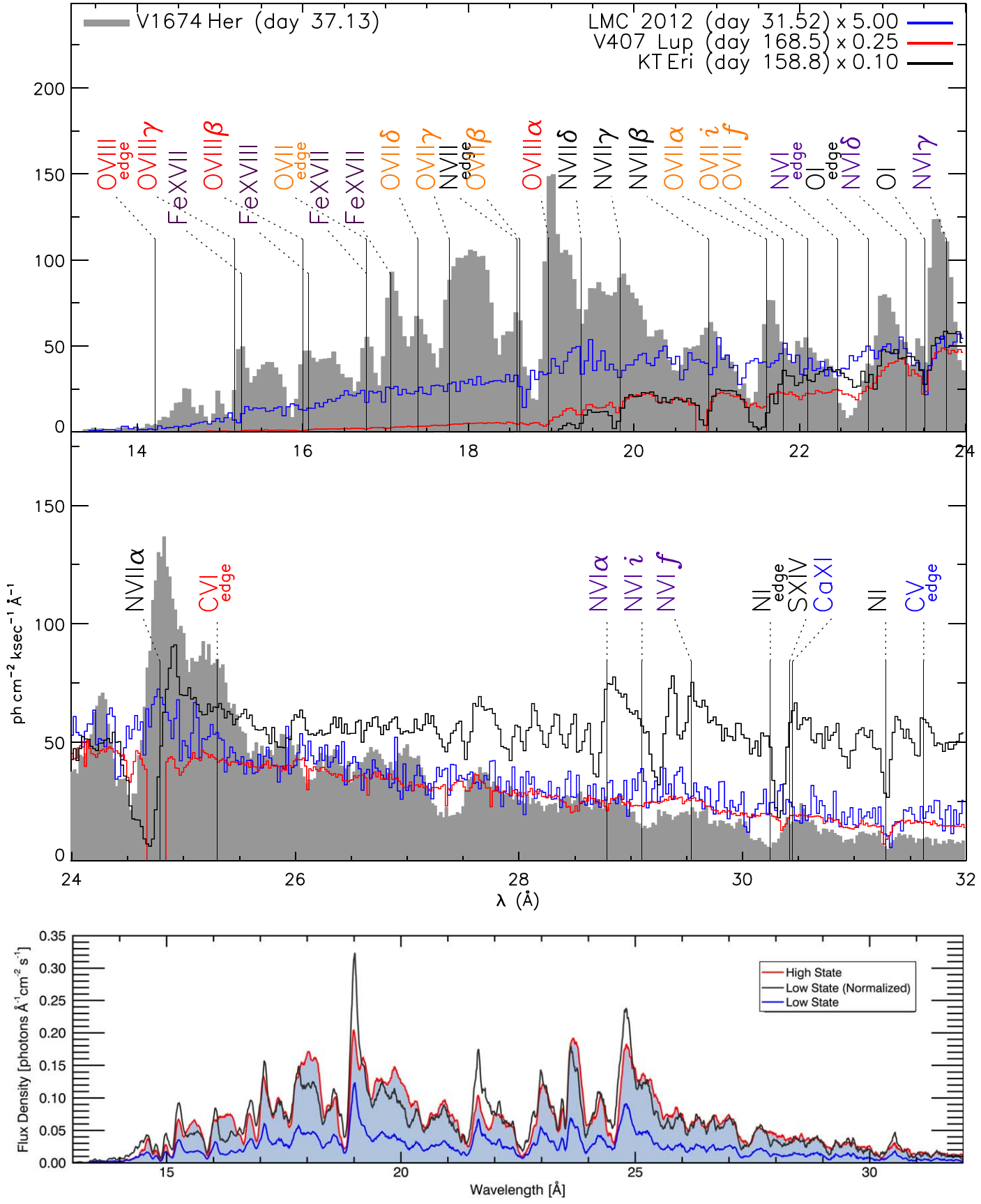

Figure 3. The Chandra LETG+HRC-S spectrum of V1674 Her. Top: rest wavelengths of prominent spectral lines are noted in different colors for the different ions, and to put V1674 Her (gray shadings) into context, overplotted are other bright nova SSS spectra. Bottom: the spectra extracted for "high" and "low" phases indicated in the phased light curve shown in Figure 2. Also shown is the "low" state spectrum renormalized to the same total flux as the "high" state spectrum.

In the case of novae, partial ionization zones of carbon and oxygen near the surface might potentially drive pulsations; this is the mechanism in the PG 1159 stars (Starrfield et al. 1984). However, the temperature of the V1674 Her WD is far hotter than the pulsating WDs and the amplitude of the oscillations is much greater than in well-known pulsating WDs (Córsico et al. 2019). Moreover, while a small change in pulsation period pre- and post-outburst appears to have occurred (Section 4.4), the enormous change in photospheric temperature and structure with such a small period change makes a g-mode pulsation explanation unlikely. We conclude that WD spin modulation, originating due to the strong magnetic field, remains the most likely explanation for the pulsed emission.

V1674 Her is then probably a member of a very small group of novae that have shown modulations in the SSS flux at the spin period of the WD. Three other novae, namely, V4743 Sgr (Ness et al. 2003; Leibowitz et al. 2006; Zemko et al. 2017; Dobrotka & Ness 2017), V2491 Cyg (Ness et al. 2011; Zemko et al. 2015), and V407 Lup (Aydi et al. 2018; Orio et al. 2021, in preparation), have shown pulsations with timescales of the order of tens of minutes during the SSS phase, and have later exhibited the same modulations in X-ray flux due to accretion at quiescence. This is typical of IPs. The transient M31 SSS described by King et al. (2002) likely belongs to the same group.

Modulation in the SSS at the WD spin period indicates the presence of either inhomogeneous surface emission, or inhomogeneous absorption. The latter might be expected from material corotating and constrained by the strong magnetic field, such as an accretion stream. A pure absorption source of modulation seems unlikely based on the wavelength-dependent pulsed fraction shown in Figure 2. The pulsed fraction is smaller toward longer wavelengths, which is opposite the trend expected for absorption unless very high ionization renders the longer wavelengths transparent.

The modulation then seems most likely due to an inhomogeneous photosphere. Such a variation in emission might potentially be caused by ongoing accretion causing temperature variations over the photospheric surface (possibly due to the burning of accreted fresh H-rich fuel), or the strong surface magnetic field affecting the photosphere and perhaps the nuclear burning shell beneath. Accretion heating is ruled out because the pulsed fraction is large and the SSS appears close to the Eddington luminosity, which is orders of magnitude higher than the accretion luminosity prior to outburst.

4.3. High-resolution SSS Spectrum

Comparisons with previous LETG+HRC-S spectra of particularly bright SSS are shown in Figure 3. The "Wien tail" high-energy cutoff in principle provides a first-order estimate of the effective temperature and indicates V1674 Her is hotter than the other novae shown, although complications due to the O VIII absorption edge in V1674 Her render the comparison more uncertain.

In the soft range, the effects of $N_{\rm H}$ dominate. We note in passing that KT Eri had lower $N_{\rm H}$, even lower than LMC 2012, while V1674 Her has a similar flux decline with wavelength to other SSS spectra with $N_{\rm H} \sim 10^{21}$ cm^{-2}.

V1674 Her has conspicuous P Cygni–like line profiles while in RS Oph, for example, absorption lines were deeper and less blueshifted. The most prominent P Cyg profile is the O VIII

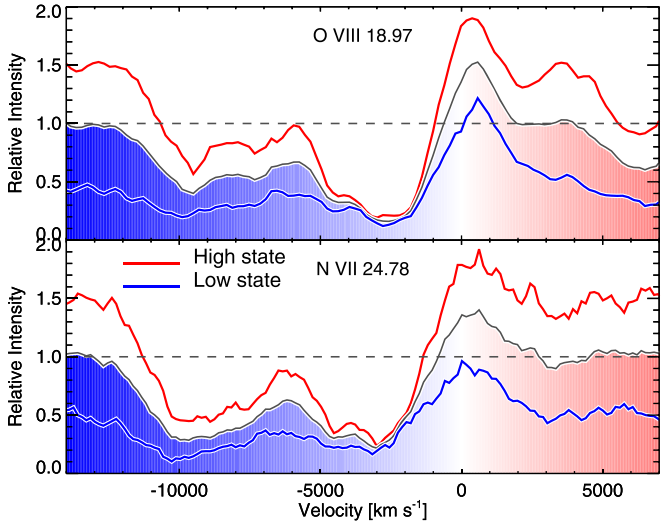

Figure 4. The Lyα lines of hydrogenic O and N demonstrating P Cygni behavior, with structured blueshifted absorption out to velocities of 11,000 km s^{-1} or so. The spectrum from the entire observation is shown (blue–red background) in addition to spectra corresponding to the "high" and "low" states.

Lyα transition near 19 Å, with the Lyβ and possibly Lyγ transitions also in evidence. The O VIII absorption lines are clearly blueshifted with respect to the labels (placed at rest wavelength), more so than in V407 Lup and KT Eri but less than in LMC 2012. The He-like O VII line is also detected at 21.6 Å with a P Cyg profile The intercombination and forbidden lines at 21.8 and 22.1 Å are not seen in emission suggesting the resonance line at 21.6 Å is photoexcited. The N VI He-like lines are not clearly detected.

The spectra show significant variations with phase. The pulsed fraction versus wavelength (Figure 2) is smallest in the cores of strong absorption lines, indicating saturation. The lower panel in Figure 3 reveals comparatively much stronger emission line components in the "low" state spectrum relative to the "high" state. Absorption features are largely similar between states. The low state has comparatively more flux shortward of about 15 Å, indicating that the temperature could be somewhat higher than in the high state.

Classic P Cyg profiles comprise an emission line component formed in a dense, radiatively driven outflow close to the stellar photosphere, while the blueshifted absorption arises because the radiation passes through the outflow material rapidly expanding in the direction of the observer. Figure 4 shows the O VIII and N VII Lyα transitions in velocity space. The emission peaks are noticeably redshifted, confirming an origin behind or within the fast outflow.

The blueshifted absorption in Figure 4 has considerable structure with two dominant components visible in both high and low states centered on velocities of approximately 3000 and 9000 km s^{-1}. These profiles demonstrate that the outflow is inhomogeneous and expanding at remarkable speeds up to 11,000 km $^{-1}$, similar to the velocity broadening seen in Balmer line profiles (e.g., Aydi et al. 2021).

4.4. Detection of a Spin Period Change of the White Dwarf?

The ZTF data (obtained pre-outburst 2018 March 26–2021 June 14) indicate an optical rotation period of $P = 501.4277 \pm 0.0002$ s (Mroz et al. 2021, and reanalysis of

those data for this work). This is different from the X-ray period derived here, $P = 501.72 \pm 0.11$ s. Similarly, the optical period of Patterson et al. (2021; post-outburst from data between 2021 July 1–August 10) of 501.52 ± 0.02 s, is significantly longer than the ZTF period and also shorter than the Chandra period.

It is tempting to interpret the periods in terms of rigid rotation and angular momentum loss resulting from the outburst. However, the Patterson et al. (2021) data straddle the Chandra observation, indicating that either X-ray and optical periods are different, or that period variations hinted at by the analysis in Section 3.1 are real. We investigate these possibilities below.

4.4.1. Period Change with Rigid Rotation

The Mroz et al. (2021) and Patterson et al. (2021) periods at face value imply a change of $\Delta P = 0.09 \pm 0.02$ s or $\Delta P/P \sim 10^{-4}$, which might be attributed to the outburst. If period drift or a QPO is not to blame, there are two mechanisms through which this might have happened: an increase in scale height of a substantial portion of the WD envelope related to the TNR and a consequent increase in moment of inertia; or the loss of mass in the explosion that carried away angular momentum.

The photospheric radius of a nova SSS is known to be expanded relative to that of the underlying WD by factors as much as 10 (e.g., Balman & Gamsızkan 2017). While the structure and mass of the expanded envelope are highly uncertain, by approximating the envelope as a spherical shell and dropping factors of approximately unity we can estimate the fractional moment of inertia change as

$$\frac{\Delta I}{I} \approx M_{\rm env}(\varepsilon^2 - 1), \tag{1}$$

where $M_{\rm env}$ is the mass of the expanded envelope in solar masses, ε is the factor of expansion of the bulk of the mass relative to the quiescent white dwarf radius, and for simplicity we have assumed a WD mass $M_{\rm WD} \approx M_\odot$ ($M_{\rm WD}$ could be as high as $1.35 M_\odot$). The envelope mass could be in the range 10^{-6}–$10^{-4} M_\odot$, depending on the accreted mass required for TNR and the amount of mixing with underlying material (e.g., Gehrz et al. 1998). Taking a large expansion factor, e.g., $\varepsilon = 5$, and assuming rigid rotation (see Section 4.4.2), fractional period changes of 10^{-4} could then potentially be explained by a simple moment of inertia change.

The angular momentum loss rate, dJ/dt, resulting from mass loss can be written (e.g., Kawaler 1988)

$$\frac{dJ}{dt} = \frac{2}{3}\frac{dM_{\rm ej}}{dt} R_{\rm WD}^2 \Omega \left(\frac{r_A}{R_{\rm WD}}\right)^n, \tag{2}$$

where $dM_{\rm ej}/dt$ is the ejected mass-loss rate, $R_{\rm WD}$ is the WD radius, n is related to the complexity of the magnetic field ($n = 2$ for a radial field and $3/7$ for a dipole in the Kawaler 1988 formalism), and r_A is the Alfvén radius, at which point the outflow exceeds the local Alfvén speed and is no longer forced to corotate by the magnetic field.

Assuming the ejected mass is a smaller fraction of the total WD mass than the fractional change in rotation period, we can ignore the change in moment of inertia of the WD due to mass loss. Further assuming for simplicity that the mass-loss rate is constant (R_A otherwise depends on $\dot{M}_{\rm ej}$), from Equation (2) conservation of angular momentum then gives

$$\frac{2}{3} M_{\rm ej} R_{\rm WD}^2 \left(\frac{r_A}{R_{\rm WD}}\right)^n = I_{\rm WD}\frac{\Delta\Omega}{\Omega}, \tag{3}$$

where $\Delta\Omega$ is the change in angular velocity. For a dipolar field ($n = 3/7$) and the observed period change, and writing $I_{\rm WD} = \alpha M_{\rm WD} R_{\rm WD}^2$ and eliminating the factor of order unity, we have for the required Alfvén radius

$$\frac{r_A}{R_{\rm WD}} \sim \left(10^{-4}\alpha \frac{M_{\rm WD}}{M_{\rm ej}}\right)^{7/3}. \tag{4}$$

For a uniform sphere, $\alpha = 0.4$, but is considerably lower for a centrally condensed WD and depends on mass. Adopting $\alpha \sim 0.2$ (e.g., Roy et al. 2021; Boshkayev et al. 2017), and for $M_{\rm WD} \approx 1 M_\odot$ the Alfvén radius is $r_A/R_{\rm WD} \sim 2 \times 10^{-5}/M_{\rm ej}$. Thus, for $r_A/R_{\rm WD}$ of order unity, the implied ejected mass is of the order of $10^{-5} M_\odot$, with the required $r_A/R_{\rm WD}$ growing rapidly for smaller ejected mass.

The Alfvén radius can also be written in terms of the surface magnetic field strength, B_0, and the mass-loss rate, $\dot{M}$, and outflow velocity, v, as (e.g., adopting Equation (4) of Kawaler 1988 to the dipole case)

$$\frac{r_A}{R_{\rm WD}} = (B_0 R_{\rm WD})^{1/2}\left(\frac{1}{\dot{M} v}\right)^{1/4}. \tag{5}$$

Combining Equations (4) and (5) and writing $\dot{M} = M_{\rm ej}/\Delta t$, with Δt being the interval over which $M_{\rm ej}$ is lost, we can determine the required surface field strength, B_0, as a function of $M_{\rm ej}$,

$$B_0 = \frac{1}{R}(10^{-4}\alpha M_{\rm WD})^{14/3}\left(\frac{v}{\Delta t}\right)^{1/2}\frac{1}{M_{\rm ej}^{25/6}}. \tag{6}$$

This is illustrated in Figure 5 for different values of $v/\Delta t$; as a reference, for an outflow at $1000\,{\rm km\,s^{-1}}$ and an ejection timescale of the order of a day ($\sim 10^5$ s), $v/\Delta t \sim 10^3$.

We noted above that, in the case of a fast nova, we might expect a low ejected mass (say $M_{\rm ej} \sim 10^{-6} M_\odot$; e.g., Gehrz et al.

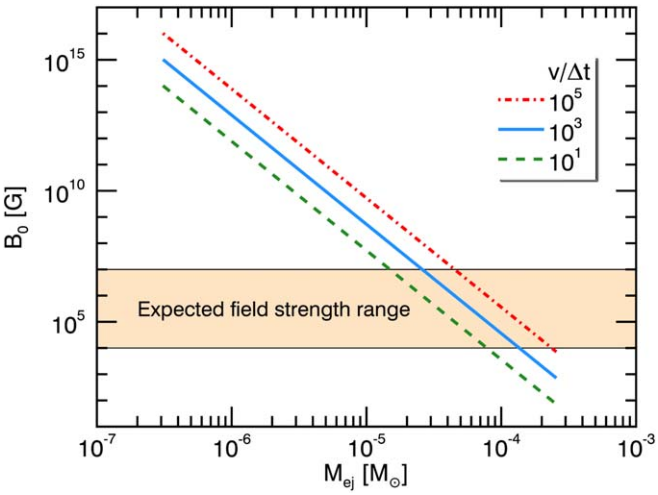

Figure 5. The WD surface magnetic field strength as a function of the ejected mass for different values of the ratio of outflow velocity at the Alfvén radius and the interval over which mass loss occurred, $v/\Delta t$.

1998). In contrast, Figure 5 demonstrates that for typical IP magnetic field strengths an ejected mass in the range 2×10^{-5}–2×10^{-4} $M_{\odot}$ is required. Such a mass is not unprecedented: Vanlandingham et al. (1996) estimated $M_{\rm ej} \sim 1.8 \times 10^{-4} M_{\odot}$ in the case of the fast nova V838 Her ($t_2 \sim 2d$).

4.4.2. Period Change with a LIMA Analogy

The difference in Patterson et al. (2021) and Chandra periods, and the possible presence of a QPO as noted in Sect 3.1, lead us to consider a third period change mechanism: that the effective photosphere post-outburst is not rigidly rotating with the underlying WD, but is at or slightly beyond r_A where the magnetic field can no longer enforce strict corotation. The optical photosphere lying closer to the WD can then have a shorter rotation period than the X-ray photosphere, and both periods could be subject to drift. The observed rotation period could also change through the outburst and SSS phase according to the mass-loss rate and changing photospheric radius, with expectation of a longer period earlier in the SSS phase when mass-loss rates in the radiatively driven outflow would be larger.

Such a mechanism is reminiscent of the Low-Inertia Magnetic Accretor (LIMA) model (Warner & Woudt 2002) in which accretion onto an equatorial belt of the WD causes the belt to vary its angular velocity when the magnetic field is insufficiently strong to enforce rigid rotation.

5. Summary

High-resolution Chandra spectroscopy and photometry reveal spectacularly strong X-ray pulsations in the SSS of Nova Her 2021 and remarkably fast outflows with two dominant velocity components at up to 11,000 km s^{-1}. Reported pre- and post-outburst optical pulsation periods are significantly different. They could potentially be explained by an expanded envelope and moment of inertia change. Instead, if interpreted in terms of angular momentum loss due to mass ejection, the optical period change implies 2×10^{-5}–2×10^{-4} $M_{\odot}$ was lost. The X-ray pulsation period, with a pulsed fraction of about 60% and a strongly varying pulse profile, appears to be longer than the reported contemporaneous post-outburst optical pulsation period, although the Chandra data are also suggestive of the presence of a QPO with period variations similar to the optical and X-ray period differences. In either case we speculate that this could be due to different X-ray and optical photospheric depths, rotating nonrigidly relative to the underlying WD.

J.J.D. was supported by NASA contract NAS8-03060 to the Chandra X-ray Center and thanks the Director, Pat Slane, for continuing advice and support. We also thank the Chandra Mission Planning group for their work that enabled this DDT observation to be executed. G.J.M.L. is member of the CIC-CONICET (Argentina) and acknowledges support from grant ANPCYT-PICT 0901/2017. D.P.K.B. is supported by a CSIR Emeritus Scientist grant-in-aid which is being hosted by the Physical Research Laboratory, Ahmedabad. K.L.P. and A.P.B. acknowledge funding from the UK Space Agency.

ORCID iDs

Jeremy J. Drake https://orcid.org/0000-0002-0210-2276
Jan-Uwe Ness https://orcid.org/0000-0003-0440-7193
Kim L. Page https://orcid.org/0000-0001-5624-2613
G. J. M. Luna https://orcid.org/0000-0002-2647-4373
Andrew P. Beardmore https://orcid.org/0000-0001-5186-5950
Marina Orio https://orcid.org/0000-0003-1563-9803
Julian P. Osborne https://orcid.org/0000-0002-1041-7542
Przemek Mróz https://orcid.org/0000-0001-7016-1692
Sumner Starrfield https://orcid.org/0000-0002-1359-6312
Dipankar P. K. Banerjee https://orcid.org/0000-0003-4896-2543
Solen Balman https://orcid.org/0000-0001-6135-1144
M. J. Darnley https://orcid.org/0000-0003-0156-3377
Y. Bhargava https://orcid.org/0000-0002-5967-8399
G. C. Dewangan https://orcid.org/0000-0003-1589-2075
K. P. Singh https://orcid.org/0000-0001-6952-3887

References

Albanese, I., Farina, A., Andreoli, V., Ochner, P., & Reguitti, A. 2021, ATel, 14718
Althaus, L. G., Gil-Pons, P., Córsico, A. H., et al. 2021, A&A, 646, A30
Aydi, E., Orio, M., Beardmore, A. P., et al. 2018, MNRAS, 480, 572
Aydi, E., Sokolovsky, K. V., Chomiuk, L., et al. 2021, ATel, 14710
Bailer-Jones, C. A. L., Rybizki, J., Fouesneau, M., Demleitner, M., & Andrae, R. 2021, AJ, 161, 147
Balam, D. D., Bohlender, D., Koubsky, P., & Labadie-Bartz, J. 2021, ATel, 14740
Balman, Ş., & Gamsızkan, Ç. 2017, A&A, 598, A129
Bellm, E. C., Kulkarni, S. R., Graham, M. J., et al. 2019, PASP, 131, 018002
Boshkayev, K., Quevedo, H., & Zhami, B. 2017, MNRAS, 464, 4349
Córsico, A. H., Althaus, L. G., Miller Bertolami, M. M., & Kepler, S. O. 2019, A&ARv, 27, 7
Dobrotka, A., & Ness, J. U. 2017, MNRAS, 467, 4865
Doherty, C. L., Gil-Pons, P., Siess, L., Lattanzio, J. C., & Lau, H. H. B. 2015, MNRAS, 446, 2599
Drake, J. J., Wagner, R. M., Starrfield, S., et al. 2003, ApJ, 584, 448
Gehrz, R. D., Truran, J. W., Williams, R. E., & Starrfield, S. 1998, PASP, 110, 3
Henze, M., Pietsch, W., Haberl, F., et al. 2014, A&A, 563, A2
Kawaler, S. D. 1988, ApJ, 333, 236
King, A. R., Osborne, J. P., & Schenker, K. 2002, MNRAS, 329, L43
Kuin, P., Starrfield, S., Orio, M., & Page, K. 2021, ATel, 14736, 1
Leibowitz, E., Orio, M., Gonzalez-Riestra, R., et al. 2006, MNRAS, 371, 424
Li, K.-L. 2021, ATel, 14707
Lomb, N. R. 1976, Ap&SS, 39, 447
Maccarone, T. J., Beardmore, A., Mukai, K., et al. 2021, ATel, 14776
Mroz, P., Burdge, K., van Roestel, J., et al. 2021, ATel, 14720
Mukai, K. 2017, PASP, 129, 062001
Munari, U., Valisa, P., & Dallaporta, S. 2021, ATel, 14704
Ness, J. U., Starrfield, S., Burwitz, V., et al. 2003, ApJL, 594, L127
Ness, J. U., Osborne, J. P., Dobrotka, A., et al. 2011, ApJ, 733, 70
Page, K. L., Beardmore, A. P., & Osborne, J. P. 2020, AdSpR, 66, 1169
Page, K. L., Orio, M., Sokolovsky, K. V., & Kuin, N. P. M. 2021, ATel, 14747
Patterson, J. 1994, PASP, 106, 209
Patterson, J., Epstein-Martin, M., Vanmunster, T., & Kemp, J. 2021, ATel, 14856
Pei, S., Luna, G. J. M., Orio, M., et al. 2021, ATel, 14798
Quimby, R. M., Shafter, A. W., & Corbett, H. 2021, RNAAS, 5, 160
Roy, S. K., Mukhopadhyay, S., & Basu, D. N. 2021, EPJP, 136, 467
Scargle, J. D. 1982, ApJ, 263, 835
Schwarz, G. J., Ness, J.-U., Osborne, J. P., et al. 2011, ApJS, 197, 31
Shugarov, S., & Afonina, M. 2021, ATel, 14835
Sokolovsky, K., Aydi, E., Chomiuk, L., et al. 2021, ATel, 14731
Starrfield, S., Bose, M., Iliadis, C., et al. 2020, ApJ, 895, 70
Starrfield, S., Cox, A. N., Kidman, R. B., & Pesnell, W. D. 1984, ApJ, 281, 800
Starrfield, S., Iliadis, C., & Hix, W. R. 2016, PASP, 128, 051001
VanderPlas, J. T. 2018, ApJS, 236, 16
Vanlandingham, K. M., Starrfield, S., Wagner, R. M., Shore, S. N., & Sonneborn, G. 1996, MNRAS, 282, 563
Wagner, R. M., Woodward, C. E., Starrfield, S., Banerjee, D. P. K., & Evans, A. 2021, ATel, 14746

Warner, B., & Woudt, P. A. 2002, MNRAS, 335, 84
Wickramasinghe, D. 2014, in EPJ Web of Conferences, Physics at the Magnetospheric Boundary, 64, ed. E. Bozzo et al., 03001
Woodward, C. E., Banerjee, D. P. K., Evans, A., Wagner, R. M., & Starrfield, S. 2021a, ATel, 14765
Woodward, C. E., Banerjee, D. P. K., Geballe, T. R., et al. 2021b, ApJL, 922, L10
Zemko, P., Mukai, K., & Orio, M. 2015, ApJ, 807, 61
Zemko, P., Orio, M., Luna, G. J. M., et al. 2017, MNRAS, 469, 476